The *Drosophila* Eukaryotic Initiation Factor eIF6 affects development by regulating apoptosis via the ecdysone pathway

Arianna Russo[1,2], Guido Gatti[1,3], Roberta Alfieri[1], Elisa Pesce[1], Kelly Soanes[4], Sara Ricciardi[1,3], Cristina Cheroni[1], Thomas Vaccari[3], Stefano Biffo[1,3]*, Piera Calamita[1,3]*

[1] INGM, National Institute of Molecular Genetics, "Romeo ed Enrica Invernizzi", Milan, Italy

[2] DiSIT, University of Eastern Piedmont, Alessandria, Italy

[3] DBS, Università degli Studi di Milano

[4] Aquatic and Crop Resource Development - National Research Council of Canada

*These authors contributed equally to this work

Address correspondence to Piera Calamita or Stefano Biffo Via Francesco Sforza 35 20122 Milano Italia. calamita@ingm.org; biffo@ingm.org

Running Title: DeIF6 regulates PCD via 20-HE

ABSTRACT

Translation factors downregulation modulates gene expression but the effect of their overexpression is still unknown. The Eukaryotic Initiation Factor 6 (eIF6) is necessary for ribosome biogenesis and translation initiation. The *eif6* gene is a single genetic locus highly conserved from yeast to humans indicating a tight regulation of its gene dosage. eIF6 haploinsufficiency protects mice from lymphomagenesis, and eIF6 is upregulated or amplified in some cancers, but a mechanistic study on the effects of eIF6 overexpression is still lacking. Taking advantage of genetic tractability of *D. melanogaster*, we characterized the first *in vivo*

model of eIF6 upregulation. *Drosophila* eIF6 overexpression increases translation and results in a *rough* eye phenotype due to aberrant apoptosis. Mechanistically, eIF6 reshapes transcription and histone acetylation, disrupting the ecdysone network. This work is the first evidence of how increased translation generates a full transcriptional and hormonal dysregulation, providing new perspectives on the physiological relevance of the translational machinery in regulating gene expression and a model to screen drugs potentially useful to treat cells with altered *eif6* gene dosage.

INTRODUCTION

Ribosomal proteins (RPs) and Eukaryotic Initiation Factors (eIFs) are necessary for the control of two major cellular processes: ribosome biogenesis and translational control [1, 2, 3, 4, 5]. Recently, it has become evident that the alteration of gene dosage in either one of these two classes of factors is causative of many pathologies, and it has been widely established that their downregulation can protect from cancer [6].

Interestingly, proteins involved in ribosome biogenesis do not usually have a role in the translational control and *vice versa* [7]. Conversely, the Eukaryotic Initiation Factor 6 (eIF6) is involved in both processes [8]. Around 20% of eIF6 is essential for nucleolar maturation of the large subunit of the ribosome, the 60s [9]. Moreover, by binding the 60S itself, eIF6 has an anti-association activity, preventing the premature joining of 60S with a 40S not loaded with a mRNA. The release of eIF6 is then required for the formation of an active 80S [10]. In mammals, eIF6 acts as a translation factor necessary for fatty acid synthesis and glycolysis through translational regulation of G/C rich or uORF containing mRNAs, such as CEBP/β, ATF4 and CEBP/δ [11, 12].

Strikingly, high levels of eIF6 or hyperphosphorylated eIF6 are observed in some cancers [13, 14], and are rate limiting for tumour onset and progression in mice [15]. In addition, eIF6 amplification is observed in luminal breast cancer patients [16]. However, whether eIF6 overexpression *per se* can change a transcriptional program in the absence of other genetic lesions is still unknown.

eIF6 is highly conserved in yeast, *Drosophila* and humans [17]. Despite ubiquitous expression, eIF6 levels *in vivo* are tightly regulated in physiological conditions, showing considerable variability of expression among different tissues [18]. During evolution, the *eif6* gene has not been subjected to gene duplication. These

observations, together with its regulatory role in ribosome biogenesis, translation, and metabolism, suggest a conserved need for strict regulation of *eif6* gene dosage. Importantly, these observations suggest that it might be difficult to generate *in vivo* models with altered eIF6 expression levels [19].

Taking advantage of the high sequence similarity among *eif6* homologues, we focused our study on the effects of eIF6 overexpression, using *Drosophila melanogaster*, an ideal model to manipulate gene expression in a time- and tissue-dependent manner using the GAL4/UAS system [20, 21]. Such *in vivo* gain of function approach allowed us to investigate how gene dosage alteration influenced the health of an organ developing within an intact organism.

Here, we used as a model organ the fly eye, whose development from epithelial primordia, the larval eye imaginal disc, is well understood. The adult fly compound eye is a stunningly beautiful structure of approximately 800 identical units, called ommatidia [22]. Each ommatidium is composed of eight neuronal photoreceptors, four glial-like cone cells and pigment cells. The study of such simple structure with the powerful genetic tools available in *Drosophila* has majorly improved our understanding of the basis of cell differentiation, apoptosis and cell-cell interactions [23, 24]. By characterizing DeIF6 overexpression we have found alterations in the formation of the adult eye, which are dependent on aberrant apoptosis during the pupal developmental stage. Interestingly, such defects correlated with an increase in general translation. Importantly, we also observed a reshaping of the eye transcriptome that revealed a coordinated downregulation of the ecdysone biosynthesis pathway, associated with decreased Histone Deacetylases (HDACs) activity. Overall, our study provides the first evidence of an increase in translation dependent on a heightened *eif6* gene dosage, that is likely to determine metabolic

86 changes and a transcriptional rewiring of a developing organ. We demonstrate that
87 the overexpression of eIF6 causes a delay and an increase in apoptosis and the
88 shutdown of hormonal signalling, providing a new and simple model to screen for
89 therapeutic molecules relevant for cancers with aberrant *eif6* gene dosage.

RESULTS

DeIF6 overexpression severely alters eye development

To study the role of DeIF6 during development we first used the *P* element allele *eIF6*^{k13214} [25]. To examine the effect of *Deif6* loss of function in mosaic animals, we induced mitotic clones homozygous for *eIF6*^{k13214} in first instar larvae by heat shock-induced FLIP/*FLP*-mediated homologous recombination [26]. We did not observe clones of mutant cells with the exception of small ones in the wing margin. Similar results were obtained in a *minute* (M) background that provides a growth advantage to mutant cells, or by targeted expression of FLP in the wing margin (Figure S1a). Together, these results indicate that eIF6 is strictly required for cell viability in *Drosophila*.

To assess the effects of the gain of function, we overexpressed *Deif6* ubiquitously using the *TubGAL4* driver. Ectopic expression resulted in late embryonic lethality (Figure S1b). To circumvent early lethality, we focused on a non-essential fly organ, the eye. DeIF6 overexpression during late eye disc development, using the *GMRGAL4* driver, caused the formation of a *rough* adult eye (Figure 1a-b). A *rough* eye is often associated with alterations in the fine structure of the compound eye [27, 28, 29, 30]. Indeed, SEM analysis showed severe disruption of the stereotypic structure of the wild-type eye, with flattened ommatidia and bristles arranged in random patterns (Figure 1c). Moreover, semithin sections evidenced that the *roughness* was not due to loss of photoreceptors, but rather to an aberrant arrangement of cells (Figure 1d). These data show that increasing DeIF6 gene dosage in the fly eye causes developmental alteration that allows the characterization of DeIF6 functions during the early events associated with its increased expression.

Increased *Deif6* gene dosage results in elevated translation

Since eIF6 plays a role in the regulation of translation by binding 60S subunits and preventing premature association into an 80S complex [14], we then asked what happens to translation *in vivo,* with increased eIF6 gene dosage. To this end, we first assessed the number of eIF6 binding sites on *Drosophila* 60S subunits using an *in vitro* Ribosome Interaction Assay (iRIA) recently developed [31]. We found that the expression of DeIF6 in larval eye discs led to 25% reduction of free 60S sites when compared to control (Figure 1e), indicating that the ectopic expressed protein was able to bind the 60S, thus retaining its functionality. Next, using a modified SUnSET assay [32], we measured translation in eye imaginal discs treated *ex vivo* with puromycin, incorporated in protein nascent chains by ribosomes. Remarkably, in the condition of DeIF6 overexpression, cells incorporate almost twice the amount of puromycin of controls (Figure 1f-g). Taken together, our biochemical experiments reveal that eIF6 overexpression reduces the free 60S pool and increases puromycin incorporation, i.e. translation.

To evaluate whether increased puromycin incorporation upon eIF6 overexpression was specific to *Drosophila*, we overexpressed human eIF6 in HEK293T cells grown upon serum stimulation and examined puromycin incorporation with a cytofluorimeter. Upon eIF6 2-fold expression relative to control (Figure S1c), we observed an increase in puromycin incorporating cells in the condition of increased eIF6 (Figure S1d-e). These data demonstrate that increased eIF6 leads to a conserved elevation of the general translational rate, both *in vivo* and in cultured cells.

DeIF6 overexpression impairs apoptosis during pupal development

To understand how deregulated protein synthesis leads to the tissue defects observed upon DeIF6 overexpression, we performed a thorough analysis of eye development. Analyzing larval eye discs revealed no differences in morphology or cell identity compared to control (Figure S2a-c). Then, we analyzed the effect of DeIF6 overexpression during pupal development. We found that at 40h after puparium formation (APF) both neuronal and cone cells were present in the correct number. Conversely, we observed that the intra/inter-ommatidial morphology was altered (Figure 2). One of the fundamental events controlling ommatidial morphology is a developmentally-controlled wave of Programmed Cell Death (PCD), sweeping the tissue from 25h to 40h APF [24]. TUNEL assay showed the absence of apoptotic nuclei at 28h APF when DeIF6 was overexpressed, whereas the *GMRGAL4/+* retinae showed many of them (Figure S3a). Thus, we analyzed the *Drosophila* effector caspase Dcp-1 by immunostaining at 40h APF. Compared to control retinae showing the presence of apoptotic cells, these were completely absent in DeIF6 overexpressing retinae (Figure 3a). Interestingly, 60h APF DeIF6 overexpressing retinae showed Dcp-1 positive cells. In contrast, 60h APF wild-type retinae did not show any apoptotic cell, confirming the end of the PCD (Figure 3b). We determined the number of Dcp-1 positive cells at 40h APF and 60h APF, revealing a striking 75% reduction in the number of apoptotic cells at 40h APF and an 80% increase in DeIF6 overexpressing retinae at 60h APF (Figure 3c).

A defect in apoptosis was confirmed by staining to detect expression of the *Drosophila* β-catenin homologue Armadillo (Figure 4). Armadillo localizes to membranes of cells surrounding photoreceptors, giving an indication of their number. At 40h APF, we observed that wild-type retinae presented the typical staining expected for Armadillo, while DeIF6 overexpressing retinae showed the presence of

extra-numerary cells around the ommatidial core (Figure 4a), in line with the possibility that these were not removed by PCD. By counting the number of cells in each ommatidium, we determined that DeIF6 overexpressing retinae possessed more than 15 cells, corresponding to approximately 30% more than that of a wild-type ommatidium (Figure S4a). Later in development, both at 60h and 72h APF, while in wild-type retinae the pattern of Armadillo was maintained, in DeIF6 overexpressing retinae Armadillo was no longer detectable (Figure 4b and S4b). This result suggests that all cells around photoreceptors might fail to terminally differentiate, perhaps due to the late surge of apoptosis upon DeIF6 overexpression. Our results demonstrate that the first developmental effect observed upon DeIF6 overexpression is a strong delay in the onset of PCD, which might be the cause of the *rough* eye phenotype.

Overexpression of DeIF6 specifically in cone and pigment cells is sufficient to alter PCD

Both cone and inter-ommatidial cells (IOCs) are responsible for the removal of extra-numerary cells to determine the correct number of ommatidial cells [33]. Thus, we overexpressed DeIF6 in either one of these two cell types, with the *spaGAL4* or *54CGAL4* drivers, respectively. Here, the overexpression of DeIF6 resulted in a *rough* eye phenotype, albeit a milder one with respect to the one observed with the *GMRGAL4* driver (Figure 5a, S5a). Semithin sections of *spa>DeIF6* adult eyes confirmed the loss of the eye structure but, similarly to the *GMR>DeIF6* phenotype, revealed that photoreceptors were unaffected (Figure 5b). Characterization of pupal *spa>DeIF6* retinae confirmed that the overexpression of DeIF6 was confined to cone cells (Figure 5c). In addition, similar to *GMR>DeIF6* retinae, the staining of the

markers ELAV and CUT demonstrated that cell identity was maintained, but that arrangement of cells on the plane of the tissue was disrupted (Figure S5b). Dcp-1 staining was completely absent in 40h APF retinae overexpressing DeIF6 specifically in the cone cells (Figure S5c) and present instead at 60h APF (Figure 5d), confirming the delay in apoptosis, observed in *GMRGAL4>DeIF6* retinae. To further confirm that the *rough* eye phenotype that we observed was strictly related to a defect in PCD, we blocked apoptosis by co-expressing DeIF6 and the Baculovirus caspase inhibitor p35, under the control of the *GMRGAL4* driver. Strikingly, we observed an almost complete suppression of the *rough* eye phenotype (Figure 5e-f). Together, these results indicate that overexpression of DeIF6 specifically in cone cell subtype is sufficient to cause the delay in PCD likely responsible for the *rough* eye phenotype.

Developmental defects associated with increased DeIF6 levels are not tissue specific

Once determined that the *rough* eye phenotype induced by DeIF6 overexpression correlated with an increase in general translation and with altered PCD during pupal development, we asked whether such defects were specific for the eye, or a more general effect associated with increased *Deif6* gene dosage. Thus, we overexpressed DeIF6 in a different epithelial organ, the wing, using the *MSGAL4* driver. Such manipulation led to complete disruption of the adult wing structure (Figure 6a). Moreover, we performed the SUnSET assay on wing imaginal discs, and as in eye discs, we observed a two-fold increase in puromycin incorporation upon DeIF6 overexpression (Figure 6b and 6c). Furthermore, DeF6 overexpression in wing discs led to a dramatic increase in apoptotic cells in the dorsal portion of the

disc (Figure 6d). These results indicate that regulation of the *Deif6* gene dosage is fundamental for the correct development of multiple organs and that ectopic expression is detrimental by inducing a marked increase in translation and apoptosis.

Gene expression analysis reveals that higher DeIF6 levels reshape transcriptome, resulting in altered ribosome maturation and ecdysone signalling

After assessing that increased DeIF6 levels in different tissues led to increased translation and apoptosis, we asked whether DeIF6 was also able to induce a transcriptional rewiring. Thus, we performed a comprehensive gene expression analysis by RNA-Seq of two distinct stages of eye development, by comparing larval eye imaginal discs and pupal retinae of *GMRGAL4/+* and *GMR>DeIF6* genotypes (Figure 7). In both developmental stages, we observed similar changes between the two genotypes, which included upregulation of genes related to ribosome biogenesis in *GMR>DeIF6* samples (File S1, Figure 7a and Figure S6a). Strikingly, GSAA analysis revealed also an increase in mRNAs of genes involved in rRNA processing (Figure S6a). These data show that eIF6 is a powerful inducer of ribosome biogenesis. Moreover, consistent with our phenotypic analysis, DeIF6 overexpressing retinae displayed upregulation of genes involved in eye development and in PCD (Figure 7 a,c and File S1). Conversely, mRNAs encoding specialized eye enzymes, such as those of pigment biosynthetic pathways, were downregulated in *GMR>DeIF6* samples (File S1), consistent with the altered adult eye morphology. Interestingly, the most changed genes associated with DeIF6 overexpression in eye imaginal discs belonged to the ecdysone pathway, with a striking downregulation in *GMR>DeIF6* samples of many genes involved in 20-HydroxyEcdysone (20-HE)

biosynthesis (Figure 7 a, b). For example, *phm*, *sad* and *nvd* (Figure S6b) were almost absent in DeIF6 overexpressing eye imaginal disc, and also early (*rbp*) and late (*ptp52f*) responsive genes belonging to the hormone signaling cascade were downregulated (File S1). These results strongly indicate the silencing of ecdysone pathway upon ectopic DeIF6 expression. Furthermore, chromosome organization gene sets were found upregulated in our larval GSAA analysis upon DeIF6 overexpression (Figure S6c, File S1). suggesting a possible effect of DeIF6 on epigenome. Thus, we decided to measure the enzymatic activity of HDACs, which remove acetyl groups from histones [34, 35], founding an interesting two-fold reduction in HDACs activity upon DeIF6 overexpression when compared to control (Figure 7d). Consistently, it has been demonstrated that transcription of ecdysone biosynthetic enzymes is under epigenetic control [36, 37]. Overall, we demonstrated that increased DeIF6 gene dosage correlates with a dramatic reduction in transcription of ecdysone biosynthesis and signaling genes as well as to a reduction of HDACs activity, providing a potential causal link between transcriptional rewiring and translation.

20-HE administration partially rescues pupal PCD defects and eye *roughness*

The observation that ecdysone biosynthesis and signaling genes were strongly downregulated upon DeIF6 overexpression led us to determine whether hormonal silencing accounted for the *GMR>DeIF6* phenotype. To assess this, we fed third instar larvae with 20-HE, and we analyzed apoptosis at 40h APF and adult eye morphology. Notably, we found a partial rescue of the apoptotic phenotype (Figure 7e). Indeed, immunofluorescence staining for Dcp-1 showed the presence of apoptotic cells in 40h APF *GMR>DeIF6* retinae treated with 20HE, while overexpressing untreated retinae did not show any Dcp-1 positive cell (Figure 7e).

Accordingly, following 20-HE treatment, we observed a partial rescue of the *rough* eye phenotype in adults. Indeed, when DeIF6 was overexpressed, eyes were 30% smaller than control. Instead, DeIF6 overexpressing larvae fed with 20-HE showed eyes 20% bigger than controls, even if still smaller respect to *GMRGAL4/+* (Figure 7f).

These data indicate that the developmental apoptotic defect and the associated *rough* eye phenotype depend on the reduction of ecdysone signaling.

DISCUSSION

We demonstrate that higher levels of eIF6 are sufficient to induce an increase in ribosome biogenesis and translation that generates a complex transcriptional and metabolic reprogramming that blocks apoptosis and causes the shutoff of hormonal production (Figure 8). Rescue of hormonal supply partly reverts apoptosis and the related developmental deficits, demonstrating that translation acts upstream of transcription and metabolism *in vivo*.

Translation is the most energy consuming process in cells [38] and thus is tightly regulated, mostly in its initiation step. Recently, many studies have highlighted how alterations in the ribosomal machinery and/or in translational control are involved in several pathologies [39]. Increased protein synthesis was often interpreted as a general by-product of increased proliferation. eIF6 has been found upregulated in many cancers, including mesothelioma, breast and colorectal cancer [13, 16, 40]. Conversely, eIF6-haploinsufficiency protects mice from lymphomagenesis in an Eμ-Myc model [15]. In our eIF6 overexpressing model, we observe an increase in mRNAs encoding for rRNA processing factors, suggesting that ribosome biogenesis is upregulated when eIF6 levels are heightened. Interestingly, we also show that the overexpression of DeIF6 causes a two-fold increase in general translation both in the developing eye and wing. These data show that *in vivo* eIF6 can act in a feed-forward loop that amplifies the efficiency of the translational machinery, and suggest that its upregulation may provide an advantage to cancer cells, through an upregulation of both ribosome biogenesis and general translation.

How could an increase in translation dictated by excess eIF6 impact tumour cell fate? A clue to this is represented by the inhibition of physiological PCD in the fly eye during the pupal stage [33] upon DeIF6 overexpression, as previously observed in *X.*

laevis [41]. Such changes in apoptosis are mirrored in our transcriptome analysis. We performed two independent gene expression analyses, in two distinct developmental windows: the first in the larva, to appreciate the early events associated with DeIF6 overexpression, the latter in the mid-pupal stage when we observed the apoptotic defect, which reveals an upregulation of apoptotic genes in overexpressing eyes. We observe that DeIF6 causes a delay and an increase in PCD, that is in itself responsible for the *rough* eye phenotype. Overall, the effects of the manipulation of DeIF6 levels result in a change in apoptosis that is therefore explained by transcriptional changes. This observation means that protein synthesis can acquire a driver role in transcription.

In summary, our data are consistent with two possibilities: developmental PCD could be delayed by excess DeIF6. Alternatively, PCD could be repressed at the correct developmental time and apoptotic elimination of defective cells overexpressing DeIF6 could be triggered later independently of developmental signals. The fact that overexpression of DeIF6 in wing discs, which are not subjected to developmental apoptosis, leads to cell death supports the latter hypothesis. Overall, these considerations indicate that the advantage provided by excess DeIF6 to tumour cells might initially consist in escape from apoptotic clearance, but eventually, tumour cells might need to be protected from the deleterious effects of DeIF6 overexpression.

We have experimentally defined the molecular sequence of events that precede and follow the inhibition of apoptosis upon DeIF6 overexpression in eye discs. We found that an upregulation of general translation causes a gross change in the transcriptome that has a coordinated impact on biological processes, including apoptosis. Importantly, gene expression analysis performed in the larvae strongly argues for reduced ecdysone biosynthesis and signaling and 20-HE treatment leads

to a partial rescue of the pupal apoptotic defect and consequently of the *rough* eye phenotype. Therefore, our data place DeIF6 upstream of ecdysone regulation, that is in turn responsible for the incapability of DeIF6 overexpressing retinae to undergo apoptosis in the right developmental window. It has been established that epigenetic changes control the transcription of ecdysone biosynthetic enzymes [36, 37]. We previously found that, in mammals, eIF6 haploinsufficiency caused a puzzling signature that mimicked alterations obtained by histones acetylation inhibitors [11]. Intriguingly, our larval GSAA analysis unveils that genes belonging to the chromosome organization gene set, such as *Gcn5* and *Ada1-2*, are upregulated when DeIF6 is overexpressed. Here, we show that DeIF6 expression leads to a decrease in HDACs activity. Thus, the data suggest that DeIF6 overexpression causes a transcriptional reshaping that leads to complex epigenetic changes which in turn prevent the transcription of mRNAs of the ecdysone biosynthetic pathway. This new mechanistic effect extends the previous observation that demonstrated the role of eIF6 in the translation of uORFs containing mRNAs [11, 42]. Curiously, an HTS screening for modulators of chromatin structure, years ago identified as a major player another initiation factor, eIF3h [43].

In summary, our study demonstrates that overexpression of eIF6 in developing organs is sufficient to induce an increase in ribosome biogenesis and translation that correlates with a complex transcriptional and metabolic changes leading to apoptotic and hormonal defects. Rescue of apoptosis defect and the related developmental deficits by hormone supplementation indicates that eIF6 activity on ribosome biogenesis and translation control is likely the cause of transcriptional and metabolic changes that induce the phenotype *in vivo* (Figure 8). It will be interesting to use the *Drosophila* model that we have established and presented here for *in vivo* screening

346 of compounds that suppress the effect of eIF6 overexpression to isolate useful
347 therapeutics relevant to the protumorigenic role of mammalian eIF6.

MATERIALS AND METHODS

Genetics

Fly strains were maintained on standard cornmeal food at 18°C. Genetic crosses were performed at 25°C, with the exception of *GMRGAL/+* and *GMR>deIF6*, performed at 18°C. The following fly mutant stocks have been used: *GMRGAL4/CTG* was a gift from Manolis Fanto (King's College, London); *UAS-DeIF6* was a gift from William J Brook (Alberta Children's Hospital, Calgary) [44]. Lines obtained from the Bloomington Drosophila Stock Center (BDSC): *spaGAL4* (26656), *54CGAL4* (27328), *w1118*, *UAS-p35* (5072), *UAS-mCD8GFP* (32184), *MSGAL4* (8860).

Mosaic analysis

The *DeIF6*^{k13214} mutant clones were created by *Flippase* (*FLP*) mediated mitotic recombination [26]. The *DeIF6*^{k13214} *(P(w[+mC)=lacW) eif6[k13214]ytr[k13214]) P* element allele was recombined onto the right arm of chromosome two with the homologous recombination site (FRT) at 42D using standard selection techniques. Briefly, to create the FRT *y*$^{+}$ *pwn, DeIF6*^{k13214} chromosomes, *DeIF6*^{k13214} was recombined onto the FRT chromosome originating from the *y; P{FRT}42D pwn[1] P{y+}44B/CyO* parental stock. The *yellow*$^{+}$ *pwn DeIF6*^{k13214}*G418* resistant flies were selected to create stocks for clonal analysis. Similarly, stocks used for generating unmarked *DeIF6*^{k13214} clones were created by recombining *DeIF6*^{k13214} with the 42D FRT chromosome using the *w[1118]; P{FRT}42D P{Ubi-GFP}2R/CyO* parental line. Targeted mitotic wing clones were generated by crossing flies with *UAS-FLP*, the appropriate GAL4 driver and the suitable *42D* FRT second chromosome with the *42D* FRT *DeIF6*^{k13214}. The *hs* induced *DeIF6*^{k13214} mitotic clones were created by

following standard techniques. Briefly, 24 and 48 hours larvae with the appropriate genotypes were heat shocked for 1 hour at 37°C followed by incubation at 25°C.

Cell culture and transfections

HEK293T cells were grown in DMEM (Lonza, Basel, Switzerland) supplemented with 10% Fetal Bovine Serum (FBS) and 1% penicillin, streptomycin, L-glutamine (Gibco, Waltham, MA, USA) and maintained at 37°C and 5% CO_2. Mycoplasma testing was performed before experiments. Cells were transfected with pcDNA3.1-eIF6 [19], or an empty vector, with Lipofectamine® 2000 (Invitrogen, Carlsbad, CA, USA, #11668019) following manufacturer protocol.

RNA isolation and RNA sequencing

Total RNA was extracted with mirVana™ isolation kit according to the manufacturer protocols (ThermoFisher Scientific, Waltham, MA, USA, #AM 1560) from 10 eye imaginal discs (larval stage) or 10 retinae (pupal stage). RNA quality was controlled with BioAnalyzer (Agilent, Santa Clara, CA, USA). Libraries for Illumina sequencing were constructed from 100 ng of total RNA with the Illumina TruSeq RNA Sample Preparation Kit v2 (Set A) (Illumina, San Diego, CA, USA). The generated libraries were loaded on to the cBot (Illumina) for clustering on a HiSeq Flow Cell v3. The flow cell was then sequenced using a HiScanSQ (Illumina). A paired-end (2×101) run was performed using the SBS Kit v3 (Illumina). Sequence deepness was at 35 million reads.

Bioinformatic Analysis

Read pre-processing and mapping

Three biological replicates were analyzed for *GMRGAL4/+* and *GMR>DeIF6* larval eye imaginal discs and four biological replicates were analyzed for *GMRGAL4/+* and *GMR>DeIF6* pupal retinae, for a total of 14 samples. Raw reads were checked for quality by FastQC software (version 0.11.2, S., A. FastQC: a quality control tool for high-throughput sequence data. 2010; Available from: http://www.bioinformatics.babraham.ac.uk/projects/fastqc), and filtered to remove low quality calls by Trimmomatic (version 0.32) [45] using default parameters and specifying a minimum length of 50. Processed reads were then aligned to *Drosophila melanogaster* genome assembly GRCm38 (Ensembl version 79) with STAR software (version 2.4.1c) [46].

Gene expression quantification and differential expression analysis.

HTSeq-count algorithm (version 0.6.1, option -s = no, gene annotation release 79 from Ensembl) [47] was employed to produce gene counts for each sample. To estimate differential expression, the matrix of gene counts produced by HTSeq was analyzed by DESeq2 (version DESeq2_1.12.4) [48].

The differential expression analysis by the DeSeq2 algorithm was performed on the entire dataset composed by both larvae and pupae samples. The two following comparisons were analyzed: *GMR>DeIF6 versus GMRGAL4/+* larval eye imaginal discs (6 samples overall) and *GMR>DeIF6 versus GMRGAL4/+* pupal retinae (8 samples in total). Reads counts were normalized by calculating a size factor, as implemented in DESeq2. Independent filtering procedure was then applied, setting the threshold to the 62 percentile; 10886 genes were therefore tested for differential expression.

Significantly modulated genes in *GMR>DeIF6* genotype were selected by considering a false discovery rate lower than 5%.

Regularized logarithmic (rlog) transformed values were used for heat map representation of gene expression profiles.

Analyses were performed in R version 3.3.1 (2016-06-21, Computing, T.R.F.f.S. R: A Language and Environment for Statistical Computing. Available from: http://www.R-project.org/).

Functional analysis by topGO

The Gene Ontology enrichment analysis was performed using topGO R Bioconductor package (version topGO_2.24.0). The option *nodesize = 5* is used to prune the GO hierarchy from the terms which have less than 5 annotated genes and the *annFUN.db* function is used to extract the gene-to-GO mappings from the genome-wide annotation library *org.Dm.eg.db* for *D. melanogaster*. The statistical enrichment of GO was tested using the Fisher's exact test. Both the "classic" and "elim" algorithms were used.

Gene set association analysis

Gene set association analysis for larvae and pupae samples was performed by GSAA software (version 2.0) [49]. Raw reads for 10886 genes identified by Entrez Gene ID were analyzed by GSAASeqSP, using gene set C5 (*Drosophila* version retrieved from http://www.go2msig.org/cgi-bin/prebuilt.cgi?taxid=7227) and specifying as permutation type 'gene set' and as gene set size filtering min 15 and max 800.

Western blotting and antibodies

Larval imaginal discs, pupal retinae and adult heads were dissected in cold Phosphate Buffer Saline (Na_2HPO_4 10 mM, KH_2PO_4 1.8 mM, NaCl 137 mM, KCl 2.7 mM, pH 7.4) (PBS) and then homogenized in lysis buffer (HEPES 20 mM, KCl 100

mM, Glycerol 5%, EDTA pH 8.0 10 mM, Triton-X 0.1%, DTT 1mM) freshly supplemented with Protease Inhibitors (Sigma, St. Louis, MO, USA, #P8340). Protein concentration was determined by BCA analysis (Pierce, Rockford, IL, USA, #23227). Equal amounts of proteins were loaded and separated on a 10% SDS-PAGE, then transferred to a PVDF membrane. Membranes were blocked in 10% Bovine Serum Albumin (BSA) in PBS-Tween (0.01%) for 30 minutes at 37°C. The following primary antibodies were used: rabbit anti-eIF6 (1:500, this study), rabbit anti-β-actin (1:4000, CST, Danvers, MA, USA, #4967). To produce the anti-eIF6 antibody used in this study, a rabbit polyclonal antiserum against two epitopes on COOH-terminal peptide of eIF6 (NH2-CLSFVGMNTTATEI-COOH eIF6 203-215 aa; NH2-CATVTTKLRAALIEDMS-COOH eIF6 230-245 aa) was prepared by PrimmBiotech (Milan, Italy, Ab code: 201212-00003 GHA/12), purified in a CNBr-Sepharose column and tested for its specificity against a mix of synthetic peptides with ELISA test. The following secondary antibodies were used: donkey anti-mouse IgG HRP (1:5000, GE Healthcare, Little Chalfont, UK, Amersham #NA931) and donkey anti-rabbit IgG HRP (1:5000, GE Healthcare, Amersham #NA934).

SUnSET Assay

Larval imaginal eye and wing discs were dissected in complete Schneider medium (Lonza, Basel, Switzerland) and treated *ex vivo* with puromycin (50 µg/mL) for 30 minutes at room temperature, then fixed in 3% paraformaldehyde (PFA) for 1 hour at room temperature. Immunofluorescences were then performed as described below, using a mouse anti Puromycin (1:500, Merck Millipore, Billerica, MA, USA, #MABE343) as a primary antibody. Discs were then examined by confocal microscope (Leica SP5, Leica, Wetzlar, Germany) and fluorescence intensity was

measured with ImageJ software. For protein synthesis measurement in HEK293T cells, after 48 hours of transfection with the pcDNA3.1-eIF6 or the empty vector, we followed the adapted SUnSET protocol described in [50]. All experiments were performed at least three times, in triplicate.

Cells count

GMRGAL4/+ and *GMR>DeIF6* pupal retinae at 40h APF were dissected, fixed, and stained with anti-Armadillo to count cells, as previously described [51]. Cells contained within a hexagonal array (an imaginary hexagon that connects the centres of the surrounding six ommatidia) were counted; for different genotypes, the number of cells per hexagon was calculated by counting cells, compared with corresponding control. Cells at the boundaries between neighbouring ommatidia count half. At least 3 hexagons (equivalent to 9 full ommatidia) were counted for each genotype, and phenotypes were analysed. Standard Deviation (SD) was used as statistical analysis.

Immunofluorescences, antibodies and TUNEL Assay

Larval imaginal discs and pupal retinae were dissected in cold PBS and fixed in 3% paraformaldehyde (PFA) for 1 hour at room temperature, then washed twice with PBS and blocked in PBTB (PBS, Triton 0.3%, 5% Normal Goat Serum and 2% Bovine Serum Albumin) for 3 hours at room temperature. Primary antibodies were diluted in PBTB solution and incubated O/N at 4°C. After three washes with PBS, tissues were incubated O/N at 4°C with secondary antibodies and DAPI (1:1000, Molecular Probes, Eugene, OR, USA, #D3571) in PBS. After three washes with PBS, eye imaginal discs and retinae were mounted on slides with ProLong Gold (LifeTechnologies, Carlsbad, CA, USA, #P36930). The following primary antibodies

were used: rabbit anti-eIF6 (1:50, this study), rat anti-ELAV (1:100, Developmental Study Hybridoma Bank DSHB, Iowa City, IA, USA, #7E8A10), mouse anti-CUT (1:100, DSHB, #2B10), mouse anti-Rough (1:100, DSHB, #ro-62C2A8), mouse anti-Armadillo (1:100, DSHB, #N27A), mouse anti-Chaoptin (1:100, DSHB, #24B10), rabbit anti- Dcp-1 (1:50, CST, #9578), mouse anti-Puromycin (1:500, Merck Millipore, #MABE343). The following secondary antibodies were used: donkey anti-rat, donkey anti-mouse, donkey anti-rabbit (1:500 Alexa Fluor® secondary antibodies, Molecular Probes). Dead cells were detected using the In Situ Cell Death Detection Kit TMR Red (Roche, Basel, Switzerland, #12156792910) as manufacturer protocol, with some optimization. Briefly, retinae of the selected developmental stage were dissected in cold PBS and fixed with PFA 3% for 1 hour at room temperature. After three washes in PBS, retinae were permeabilized with Sodium Citrate 0.1%-Triton-X 0.1% for 2 minutes at 4°C and then incubated overnight at 37°C with the enzyme mix. Retinae were then rinsed three times with PBS, incubated with DAPI to stain nuclei and mounted on slides. Discs and retinae were examined by confocal microscopy (Leica SP5) and analysed with Volocity 6.3 software (Perkin Elmer, Waltham, MA, USA). All immunofluorescences were performed at least on three independent experiments.

Semithin sections

Semithin sections were prepared as described in [52]. Adult eyes were fixed in 0.1 M Sodium Phosphate Buffer, 2% glutaraldehyde, on ice for 30 min, then incubated with 2% OsO4 in 0.1 M Sodium Phosphate Buffer for 2 hours on ice, dehydrated in ethanol (30%, 50%, 70%, 90%, and 100%) and twice in propylene oxide. Dehydrated eyes were then incubated O/N in 1:1 mix of propylene oxide and epoxy resin (Sigma,

Durcupan™ ACM). Finally, eyes were embedded in pure epoxy resin and baked O/N at 70°C. The embedded eyes were cut on a Leica UltraCut UC6 microtome using a glass knife and images were acquired with a 100X oil lens, Nikon Upright XP61 microscope (Nikon, Tokyo, Japan).

Ecdysone treatment

For ecdysone treatment, 20-HydroxyEcdysone (20HE) (Sigma, #H5142) was dissolved in 100% ethanol to a final concentration of 5 mg/mL; third instar larvae from different genotypes (*GMRGAL4/+* and *GMR>DeIF6*) were collected and placed in individual vials on fresh standard cornmeal food supplemented with 240 µg/mL 20-HE. Eye phenotype was analyzed in adult flies, and images were captured with a TOUPCAM™ Digital camera. Eye images were analyzed with ImageJ software.

In vitro Ribosome Interaction Assay (iRIA)

iRIA assay was performed as described in [31]. Briefly, 96-well plates were coated with a cellular extract diluted in 50 µL of PBS, 0.01% Tween-20, O/N at 4°C in humid chamber. Coating solution was removed and aspecific sites were blocked with 10% BSA, dissolved in PBS, 0.01% Tween-20 for 30 minutes at 37 °C. Plates were washed with 100 µL/well with PBS-Tween. 0.5 µg of recombinant biotinylated eIF6 were resuspended in a reaction mix: 2.5 mM $MgCl_2$, 2% DMSO and PBS-0.01% Tween, to reach 50 µL of final volume/well, added to the well and incubated with coated ribosomes for 1 hour at room temperature. To remove unbound proteins, each well was washed 3 times with PBS, 0.01% Tween-20. HRP-conjugated streptavidin was diluted 1:7000 in PBS, 0.01% Tween-20 and incubated in the well, 30 minutes at room temperature, in a final volume of 50 µL. Excess of streptavidin

was removed through three washes with PBS-Tween. OPD (o-phenylenediamine dihydrochloride) was used according to the manufacturer's protocol (Sigma-Aldrich) as a soluble substrate for the detection of streptavidin peroxidase activity. The signal was detected after the incubation, plates were read at 450 nm on a multiwell plate reader (Microplate model 680, Bio-Rad, Hercules, CA, USA). This experiment was performed at least three times, in triplicate.

HDACs activity

HDACs activity was measured with the fluorometric HDAC Activity Assay kit (Sigma, #CS1010-1KT) according to the manufacturer's instructions. Briefly, cells were lysed with a buffer containing 50 mM HEPES, 150 mM NaCl, and 0.1% Triton X-100 supplemented with fresh protease inhibitors. 20 µg of cell lysates were incubated with assay buffer containing the HDACs substrate for 30 minutes at 30°C. The reaction was terminated, and the fluorescence intensity was measured in a fluorescence plate reader with Ex. = 350-380 nm and Em. = 440-460 nm.

Statistical Analysis

Each experiment was repeated at least three times, as biological replicates; means and standard deviations between different experiments were calculated. Statistical *p*-values obtained by Student *t-test* were indicated: three asterisks *** for *p*-values less than 0.001, two asterisks ** for *p*-values less than 0.01 and one asterisks * for *p*-values less than 0.05.

ACCESSION NUMBER

ArrayExpress ID will be provided upon acceptance for publication.

FUNDING

This work was supported by ERC TRANSLATE 338999 and FONDAZIONE CARIPLO to SB.

ACKNOWLEDGEMENTS

We thank William Brook (Alberta Children's Hospital, Calgary) for UASdeif6 stocks and Manolis Fanto (King's College, London) for stocks and suggestions. We thank Valeria Berno for imaging help and Vera Giulia Volpi for semithin sections preparation.

The authors declare no competing interests.

Supplementary Information is available at Cell Death and Differentiation website

REFERENCES

1. Hershey JW, Sonenberg N, Mathews MB. Principles of translational control: an overview. *Cold Spring Harb Perspect Biol* 2012, **4**(12).

2. Kressler D, Hurt E, Bassler J. A Puzzle of Life: Crafting Ribosomal Subunits. *Trends Biochem Sci* 2017, **42**(8)**:** 640-654.

3. Kressler D, Linder P, de La Cruz J. Protein trans-acting factors involved in ribosome biogenesis in Saccharomyces cerevisiae. *Mol Cell Biol* 1999, **19**(12)**:** 7897-7912.

4. Venema J, Tollervey D. Ribosome synthesis in Saccharomyces cerevisiae. *Annu Rev Genet* 1999, **33:** 261-311.

5. Warner JR, Vilardell J, Sohn JH. Economics of ribosome biosynthesis. *Cold Spring Harb Symp Quant Biol* 2001, **66:** 567-574.

6. Robichaud N, Sonenberg N. Translational control and the cancer cell response to stress. *Curr Opin Cell Biol* 2017, **45:** 102-109.

7. Miluzio A, Beugnet A, Volta V, Biffo S. Eukaryotic initiation factor 6 mediates a continuum between 60S ribosome biogenesis and translation. *EMBO Rep* 2009, **10**(5)**:** 459-465.

8. Brina D, Miluzio A, Ricciardi S, Biffo S. eIF6 anti-association activity is required for ribosome biogenesis, translational control and tumor progression. *Biochim Biophys Acta* 2015, **1849**(7)**:** 830-835.

9. Gandin V, Miluzio A, Barbieri AM, Beugnet A, Kiyokawa H, Marchisio PC*, et al.* Eukaryotic initiation factor 6 is rate-limiting in translation, growth and transformation. *Nature* 2008, **455**(7213)**:** 684-688.

10. Ceci M, Gaviraghi C, Gorrini C, Sala LA, Offenhauser N, Marchisio PC*, et al.* Release of eIF6 (p27BBP) from the 60S subunit allows 80S ribosome assembly. *Nature* 2003, **426**(6966)**:** 579-584.

11. Brina D, Miluzio A, Ricciardi S, Clarke K, Davidsen PK, Viero G*, et al.* eIF6 coordinates insulin sensitivity and lipid metabolism by coupling translation to transcription. *Nat Commun* 2015, **6:** 8261.

12. Miluzio A, Ricciardi S, Manfrini N, Alfieri R, Oliveto S, Brina D*, et al.* Translational control by mTOR-independent routes: how eIF6 organizes metabolism. *Biochem Soc Trans* 2016, **44**(6)**:** 1667-1673.

13. Miluzio A, Oliveto S, Pesce E, Mutti L, Murer B, Grosso S*, et al.* Expression and activity of eIF6 trigger malignant pleural mesothelioma growth in vivo. *Oncotarget* 2015, **6**(35)**:** 37471-37485.

14. Sanvito F, Piatti S, Villa A, Bossi M, Lucchini G, Marchisio PC*, et al.* The beta4 integrin interactor p27(BBP/eIF6) is an essential nuclear matrix protein involved in 60S ribosomal subunit assembly. *J Cell Biol* 1999, **144**(5)**:** 823-837.

15. Miluzio A, Beugnet A, Grosso S, Brina D, Mancino M, Campaner S*, et al.* Impairment of cytoplasmic eIF6 activity restricts lymphomagenesis and tumor progression without affecting normal growth. *Cancer Cell* 2011, **19**(6)**:** 765-775.

16. Gatza ML, Silva GO, Parker JS, Fan C, Perou CM. An integrated genomics approach identifies drivers of proliferation in luminal-subtype human breast cancer. *Nat Genet* 2014, **46**(10)**:** 1051-1059.

17. Biffo S, Sanvito F, Costa S, Preve L, Pignatelli R, Spinardi L*, et al.* Isolation of a novel beta4 integrin-binding protein (p27(BBP)) highly expressed in epithelial cells. *J Biol Chem* 1997, **272**(48)**:** 30314-30321.

18. Donadini A, Giodini A, Sanvito F, Marchisio PC, Biffo S. The human ITGB4BP gene is constitutively expressed in vitro, but highly modulated in vivo. *Gene* 2001, **266**(1-2)**:** 35-43.

19. Benelli D, Cialfi S, Pinzaglia M, Talora C, Londei P. The translation factor eIF6 is a Notch-dependent regulator of cell migration and invasion. *PLoS One* 2012, **7**(2)**:** e32047.

20. Brand AH, Perrimon N. Targeted gene expression as a means of altering cell fates and generating dominant phenotypes. *Development* 1993, **118**(2)**:** 401-415.

21. del Valle Rodriguez A, Didiano D, Desplan C. Power tools for gene expression and clonal analysis in Drosophila. *Nat Methods* 2011, **9**(1)**:** 47-55.

22. Kumar JP. Building an ommatidium one cell at a time. *Dev Dyn* 2012, **241**(1)**:** 136-149.

23. Cagan RL, Reh TA. Preface. Aspects of eye development: advances over the past twenty years. *Curr Top Dev Biol* 2010, **93:** xi-xii.

24. Ready DF, Hanson TE, Benzer S. Development of the Drosophila retina, a neurocrystalline lattice. *Dev Biol* 1976, **53**(2)**:** 217-240.

25. Spradling AC, Stern D, Beaton A, Rhem EJ, Laverty T, Mozden N*, et al.* The Berkeley Drosophila Genome Project gene disruption project: Single P-element insertions mutating 25% of vital Drosophila genes. *Genetics* 1999, **153**(1)**:** 135-177.

26. Harrison DA, Perrimon N. Simple and efficient generation of marked clones in Drosophila. *Curr Biol* 1993, **3**(7)**:** 424-433.

27. Basler K, Hafen E. Specification of cell fate in the developing eye of Drosophila. *Bioessays* 1991, **13**(12)**:** 621-631.

28. Tomlinson A, Bowtell DD, Hafen E, Rubin GM. Localization of the sevenless protein, a putative receptor for positional information, in the eye imaginal disc of Drosophila. *Cell* 1987, **51**(1)**:** 143-150.

29. Tomlinson A, Kimmel BE, Rubin GM. rough, a Drosophila homeobox gene required in photoreceptors R2 and R5 for inductive interactions in the developing eye. *Cell* 1988, **55**(5)**:** 771-784.

30. Van Vactor DL, Jr., Cagan RL, Kramer H, Zipursky SL. Induction in the developing compound eye of Drosophila: multiple mechanisms restrict R7 induction to a single retinal precursor cell. *Cell* 1991, **67**(6)**:** 1145-1155.

31. Pesce E, Minici C, Babetaler J, Hurt E, Degano M, Calamita P*, et al.* Direct and high throughput (HT) interactions on the ribosomal surface by iRIA. *Sci Rep* 2015, **5:** 15401.

32. Schmidt EK, Clavarino G, Ceppi M, Pierre P. SUnSET, a nonradioactive method to monitor protein synthesis. *Nat Methods* 2009, **6**(4)**:** 275-277.

33. Rusconi JC, Hays R, Cagan RL. Programmed cell death and patterning in Drosophila. *Cell Death Differ* 2000, **7**(11)**:** 1063-1070.

34. Buchwald M, Kramer OH, Heinzel T. HDACi--targets beyond chromatin. *Cancer Lett* 2009, **280**(2)**:** 160-167.

35. de Ruijter AJ, van Gennip AH, Caron HN, Kemp S, van Kuilenburg AB. Histone deacetylases (HDACs): characterization of the classical HDAC family. *Biochem J* 2003, **370**(Pt 3)**:** 737-749.

36. Borsos BN, Pankotai T, Kovacs D, Popescu C, Pahi Z, Boros IM. Acetylations of Ftz-F1 and histone H4K5 are required for the fine-tuning of ecdysone biosynthesis during Drosophila metamorphosis. *Dev Biol* 2015, **404**(1)**:** 80-87.

37. Pankotai T, Popescu C, Martin D, Grau B, Zsindely N, Bodai L*, et al.* Genes of the ecdysone biosynthesis pathway are regulated by the dATAC histone acetyltransferase complex in Drosophila. *Mol Cell Biol* 2010, **30**(17)**:** 4254-4266.

38. Buttgereit F, Brand MD. A hierarchy of ATP-consuming processes in mammalian cells. *Biochem J* 1995, **312 (Pt 1):** 163-167.

39. Shenoy N, Kessel R, Bhagat TD, Bhattacharyya S, Yu Y, McMahon C*, et al.* Alterations in the ribosomal machinery in cancer and hematologic disorders. *J Hematol Oncol* 2012, **5:** 32.

40. Sanvito F, Vivoli F, Gambini S, Santambrogio G, Catena M, Viale E*, et al.* Expression of a highly conserved protein, p27BBP, during the progression of human colorectal cancer. *Cancer Res* 2000, **60**(3)**:** 510-516.

41. De Marco N, Iannone L, Carotenuto R, Biffo S, Vitale A, Campanella C. p27(BBP)/eIF6 acts as an anti-apoptotic factor upstream of Bcl-2 during Xenopus laevis development. *Cell Death Differ* 2010, **17**(2)**:** 360-372.

42. Ricciardi S, Miluzio A, Brina D, Clarke K, Bonomo M, Aiolfi R*, et al.* Eukaryotic translation initiation factor 6 is a novel regulator of reactive oxygen species-dependent megakaryocyte maturation. *J Thromb Haemost* 2015, **13**(11)**:** 2108-2118.

43. Daxinger L, Oey H, Apedaile A, Sutton J, Ashe A, Whitelaw E. A forward genetic screen identifies eukaryotic translation initiation factor 3, subunit H (eIF3h), as an enhancer of variegation in the mouse. *G3 (Bethesda)* 2012, **2**(11)**:** 1393-1396.

44. Ji Y, Shah S, Soanes K, Islam MN, Hoxter B, Biffo S*, et al.* Eukaryotic initiation factor 6 selectively regulates Wnt signaling and beta-catenin protein synthesis. *Oncogene* 2008, **27**(6)**:** 755-762.

45. Bolger AM, Lohse M, Usadel B. Trimmomatic: a flexible trimmer for Illumina sequence data. *Bioinformatics* 2014, **30**(15)**:** 2114-2120.

46. Dobin A, Davis CA, Schlesinger F, Drenkow J, Zaleski C, Jha S*, et al.* STAR: ultrafast universal RNA-seq aligner. *Bioinformatics* 2013, **29**(1)**:** 15-21.

47. Anders S, Pyl PT, Huber W. HTSeq--a Python framework to work with high-throughput sequencing data. *Bioinformatics* 2015, **31**(2)**:** 166-169.

48. Love MI, Huber W, Anders S. Moderated estimation of fold change and dispersion for RNA-seq data with DESeq2. *Genome Biol* 2014, **15**(12)**:** 550.

49. Xiong Q, Mukherjee S, Furey TS. GSAASeqSP: a toolset for gene set association analysis of RNA-Seq data. *Sci Rep* 2014, **4:** 6347.

50. Calamita P, Miluzio A, Russo A, Pesce E, Ricciardi S, Khanim F*, et al.* SBDS-Deficient Cells Have an Altered Homeostatic Equilibrium due to Translational Inefficiency Which Explains their Reduced Fitness and Provides a Logical Framework for Intervention. *PLoS Genet* 2017, **13**(1)**:** e1006552.

51. Cordero J, Jassim O, Bao S, Cagan R. A role for wingless in an early pupal cell death event that contributes to patterning the Drosophila eye. *Mech Dev* 2004, **121**(12)**:** 1523-1530.

52. Montrasio S, Mlodzik M, Fanto M. A new allele uncovers the role of echinus in the control of ommatidial rotation in the Drosophila eye. *Dev Dyn* 2007, **236**(10)**:** 2936-2942.

FIGURES LEGENDS

Figure 1. Increasing DeIF6 levels in the developing eye results in a *rough* eye phenotype and in an increased translation. (a) Stereomicroscope images of *GMRGAL4/+* and *GMR>DeIF6* eyes, showing a noteworthy *rough* eye phenotype. **(b)** Representative western blot showing the levels of DeIF6 expression in *GMRGAL4/+* and *GMR>DeIF6* adult eyes. **(c)** Representative SEM images of *GMRGAL4/+* and *GMR>DeIF6* adult eyes. DeIF6 overexpressing eyes have a complete aberrant morphology, showing flattened ommatidia and randomly arranged bristles. Scale bar, in order, 10 µm, 5 µm, 2.5 µm **(d)** Representative tangential sections of *GMRGAL4/+* and *GMR>DeIF6* adult eyes indicating that photoreceptors are still present in overexpressing eyes, even if their arrangement is lost. Scale bar 10 µm. **(e)** iRIA assay showing that overexpressed DeIF6 is able to bind the 60S, therefore confirming its functionality. **(f)** Quantification of SUnSET assay using ImageJ software. Graph represents mean ± SD. Statistic applied was *t-test*, paired, two tails. Experiments were performed at least three times. **(g)** Representative SUnSET assay performed using immunofluorescence experiment, indicating a two-fold increase in general translation when DeIF6 was overexpressed in eye imaginal discs. Scale bar 10 µm

785 **Figure 2. DeIF6 overexpressing retinae preserve cell identity but show an**
786 **aberrant morphology. (a)** Mid-pupal stage retinae (40h APF) stained for eIF6
787 confirming protein overexpression. **(b)** Staining for ELAV (neuronal cells marker) and
788 Cut (cone cells marker) showing that both neurons and cone cells preserve their
789 identity. Noteworthy, neural and cone cells show an incorrect arrangement on the
790 plane in association to increased DeIF6 levels. **(c)** Chaoptin (intra-photoreceptor
791 membranes marker) staining confirms the aberrant morphology of *GMR>DeIF6*
792 retinae. Scale bar 10 μm
793
794 **Figure 3. Apoptotic wave is delayed and increased when *deif6* gene dosage is**
795 **increased. (a)** Mid-pupal stage retinae (40h APF) stained for the *Drosophila*
796 caspase Dcp-1. *GMRGAL4/+* retinae show Dcp-1 positive cells, indicating that
797 Programmed Cell Death (PCD) is ongoing at this developmental stage. On the
798 contrary, *GMR>DeIF6* retinae do not show Dcp-1 positive cells, indicating a block in
799 PCD. **(b)** Late-pupal stage (60h APF) retinae stained for the *Drosophila* caspase
800 Dcp-1. *GMRGAL4/+* retinae show the absence of Dcp-1 positive cells, as expected
801 (PCD already finished at this developmental stage). On the contrary, *GMR>DeIF6*
802 retinae, show Dcp-1 positive cells, indicating a delay in PCD associated to more
803 DeIF6 levels. **(c)** Dcp-1 positive cells counts indicate an overall delay and increase in
804 PCD when DeIF6 gene dosage is increased during eye development. Graph
805 represents mean ± SD. Statistic applied was *t-test*, paired, two tails. Counts were
806 performed on three independent experiments. Scale bar 10 μm
807
808 **Figure 4. Cell number is altered during pupal stage upon DeIF6 overexpression.**
809 **(a)** Mid-pupal stage (40h APF) retinae stained for Armadillo, the *Drosophila* β-catenin

homologue, showing that when DeIF6 is overexpressed there are extra-numerary cells (indicated as *) around each ommatidium. **(b)** Late-pupal stage (60h APF) retinae stained for Armadillo, showing the loss of all cells around ommatidia upon DeIF6 overexpression. Scale bar 10 μm.

Figure 5. Increasing *deif6* gene dosage only in cone cells results in a *rough* eye phenotype, that is specifically due to increased apoptosis (a-b) Overexpression of DeIF6 only in cone cells results in *rough* eye phenotype. **(a)** Representative stereomicroscope images of *spaGAL4/+* and *spa>DeIF6* eyes showing a *rough* eye phenotype. **(b)** Representative tangential sections of *spaGAL4/+* and *spa>DeIF6* adult eyes showing disruption of the structure upon DeIF6 overexpression in cone cells. **(c)** Mid-pupal stage (40h APF) retinae stained for eIF6 confirming that overexpression of DeIF6 is restricted only to cone cells. **(d)** Late-pupal stage (60h APF) retinae of *spaGAL4/+* and *spa>DeIF6* genotypes stained for Dcp-1 confirming the delayed and increased apoptosis already observed in *GMR>DeIF6* flies. (c-d) Scale bar 10 μm **(e-f)** Blocking apoptosis rescues the *rough* eye phenotype. **(e)** Representative stereomicroscope images of *GMR>DeIF6; p35* and *GMR>DeIF6* adult eyes. **(f)** Western blot showing eIF6 levels in *GMR>DeIF6; p35* and *GMR>DeIF6 eyes*. For each genotype, the densitometric ratio (DeIF6/β-actin) was analysed with ImageJ and reported.

Figure 6. Developmental defects dependent on altered *deif6* gene dosage are not tissue specific. (a) Adult wings overexpressing DeIF6 have a completely aberrant phenotype, evidencing developmental defects. **(b)** SUnSET assay quantification of an immunofluorescence experiment, indicating again a two-fold

increase in general translation when DeIF6 is overexpressed in wing discs. Graph represents mean ± SD. Statistic applied was *t-test*, paired, two tails. The experiment was performed at least three times. **(c)** Representative SUnSET assay performed using immunofluorescence experiment, indicating again a two-fold increase in general translation when DeIF6 is overexpressed in wing discs. For each genotype, two magnifications are compared: 63x (scale bar 50 μm) and, in the small squares, 252x (scale bar 10 μm). **(d)** Apoptosis is increased in wing imaginal disc expressing more DeIF6 levels. Wing discs stained for Dcp-1 and DeIF6 in control flies (*MSGAL4/+*) and in flies overexpressing DeIF6 (*MS>DeIF6*). In *MS>DeIF6* there is a striking increase in apoptotic events, compared to the control. Scale bar 50 μm

Figure 7. RNASeq analysis shows a reshaping of transcription, resulting in rRNA processing alteration and in a gene signature specific for the eye, that reveals a role of 20-HE in defective apoptosis. (a) Venn Diagram indicating genes differentially expressed in *GMR>DeIF6* larval eye imaginal discs and *GMR>DeIF6* retinae respect to controls (*GMRGAL4/+).* **(b)** The Ecdysone Biosynthetic Pathway is strikingly shut off when DeIF6 is upregulated. Heat Map representing absolute gene expression levels in *GMR>DeIF6* and *GMRGAL4/+* eye imaginal disc samples for the subset of gene sets involved in Ecdysone Biosynthesis by Gene Ontology analysis. **(c)** mRNAs involved in Programmed Cell Death and in Eye Differentiation are upregulated in *GMR>DeIF6* retinae. Heat Map representing absolute gene expression levels in *GMR>DeIF6* and *GMRGAL4/+* retinae samples for the subset of gene sets involved in Programmed Cell Death and Eye Differentiation by Gene Ontology Analysis. **(d)** High levels of DeIF6 are associated to lower HDAC activity. Representative graph showing a lower HDACs activity in association to high DeIF6

protein levels. The assay has been performed on total protein extracts from *GMRGAL4/+* and *GMR>DeIF6* adult heads. **(e-f)** 20-HE treatment partially rescue the *rough* eye phenotype and the delay in apoptosis in 40h APF retinae **(e)** Immunofluorescence images showing that 20-HE treatment (240 µg/mL in standard fly food) rescues the apoptotic delay observed in *GMR>DeIF6* 40h APF retinae. **(f)** Representative graph showing the *GMR>DeIF6* adult fly eye size with or without treatment with 20-HE. As indicated in the graph, the fly eye size is partially rescued when the hormone is added to the fly food. Graphs represent mean ± SD. Statistic applied was *t-test*, paired, two tails. Counts were performed on three independent experiments.

Figure 8. Model for DeIF6 high levels-associated changes. We demonstrated that increased levels of DeIF6 are associated to increased general translation, resulting in a transcription rewiring. RNASeq analysis confirms that altering *deif6* gene dosage modulates apoptosis during development and interestingly, reveals a shutdown of genes involved in 20-HydroxyEcdysone biosynthesis. In addition, we found an upregulation of genes related to chromatin organization.

Figure S1. Strong alteration of *deif6* gene dosage is incompatible with life and is associated to increased general translation when overexpressed in mammalian cells. (a) *DeIF6*^{k13214} mosaic analysis. (A-F) Wild type (Oregon R) wing margin and *deif6* mutant clones. (A and B) Wild type control anterior wing margin. (C and D) Wing margin clones induced in *Minute/DeIF6*^{k13214} flies according the crosses outlined in Materials and Methods. (E and F) Mutant clones induced along the wing margin by using UAS-*Flp*; *C96*-GAL4; FRT *DeIF6*^{k13214}/FRT *y+ pwn* flies. (D and F)

Arrows and arrowheads indicate *pwn DeIF63214* homozygous mutant and heterozygous *Minute* (*M/pwn DeIF6*^{k13214}) tissues, respectively. Asterisks denote *y* twin cells and the "^" highlights heterozygous wild type bristles. **(b)** Ectopic embryonic *deif6* phenotypes. (A-B) Embryonic cuticle preparations in *TubGAL4/+* (A) and *Tub>DeIF6* (B) evidencing that DeIF6 gain of function is embryonic lethal. **(c-e)** eIF6 overexpression results in translation increase in mammalian cells. **(c)** Representative western blot showing the levels of DeIF6 expression in empty vector- and eIF6-pcDNA3.1 transfected cells. **(d)** SUnSET assay quantification of FACS analysis performed on HEK293T cells showing the same increase in general translation observed in *Drosophila* eye imaginal discs. Graph represents mean ± SD. Statistic applied was *t-test*, paired, two tails. The experiment was performed at least three times. **(e)** Dot plot of FACS analysis performed in HEK293T cells of overexpressing and control cells' populations.

Figure S2. DeIF6 overexpressing eye imaginal discs preserve cell identity and morphology. (a) *GMR>DeIF6* and *GMRGAL4/+* eye imaginal discs stained for eIF6 confirm the protein overexpression. **(b)** *GMR>DeIF6* and *GMRGAL4/+* eye imaginal discs stained for ELAV (neuronal cells marker) and Cut (cone cells marker) show that both neurons and cone cells preserve their identities. **(c)** *GMR>DeIF6* and *GMRGAL4/+* eye imaginal discs stained for Rough (R2-R5 marker) show the same pattern in both genotypes. Scale bar 50 μm.

Figure S3. PCD is delayed when DeIF6 gene dosage is increased. TUNEL assay on early (28h APF) **(a)** and mid-pupal (40h APF) stages **(b)** retinae indicate that PCD

909 is blocked at these developmental stages when DeIF6 is overexpressed. Scale bar
910 50 µm.
911
912 **Figure S4. Cell number is altered during pupal stage upon DeIF6**
913 **overexpression. (a)** Comparison of cells number across two genotypes,
914 *GMRGAL4/+* and *GMR>DeIF6*, shows that there is an increase in *GMR>DeIF6*
915 respect to control. 'Δ cells per ommatidium' refers to the number of cells gained or
916 lost within a ommatidia (number of cells in hexagon divided by 3). Results in the third
917 column represent the mean ± SD. **(b)** Late-pupal stage (72h APF) retinae stained for
918 Armadillo, the *Drosophila* β-catenin homologue, showing that when DeIF6 is
919 overexpressed cells around ommatidia are lost. Scale bar 10 µm.
920
921 **Figure S5. Increasing DeIF6 gene dosage only in pigment cells or in cone cells**
922 **results in a *rough* eye phenotype and in an aberrant morphology associated to**
923 **a block in apoptosis (a)** Overexpression of DeIF6 only in pigment cells results in
924 *rough* eye phenotype. **(b)** Mid-pupal stage (40h APF) retinae of *spaGAL4/+* and
925 *spa>DeIF6* genotypes stained for ELAV and CUT confirm that neural and cone cell
926 identity is preserved, but morphology is not. **(c)** Mid-pupal stage (40h APF) retinae of
927 *spaGAL4/+* and *spa>DeIF6* genotypes stained for Dcp-1 confirm the block in
928 apoptosis already demonstrated in *GMR>DeIF6* flies. Scale bar 10 µm
929
930 **Figure S6. RNASeq analysis reveals an upregulation in genes belonging to**
931 **ribosome biogenesis and chromosome organization gene sets and a strong**
932 **downregulation of genes related to 20-HydroxyEcdysone biosynthesis. (a)**
933 Gene Set Association Analysis (GSAA) indicates a significative upregulation of

ribosomal machinery. Representative Enrichment Plots indicating a striking upregulation of genes involved in rRNA Processing and Ribosome Biogenesis in both *GMR>DeIF6* eye imaginal discs and *GMR>DeIF6* retinae respect to their controls (*GMRGAL4/+).* **(b)** 20-HydroxyEcdysone biosynthetic pathway scheme. Genes involved in 20-HE biosynthesis are strongly downregulated in *GMR>DeIF6* eye imaginal disc, respect to control. **(c)** GSAA shows an upregulation of genes related to chromosome organization gene set in *GMR>DeIF6* eye imaginal disc, respect to control.

Fig. 1

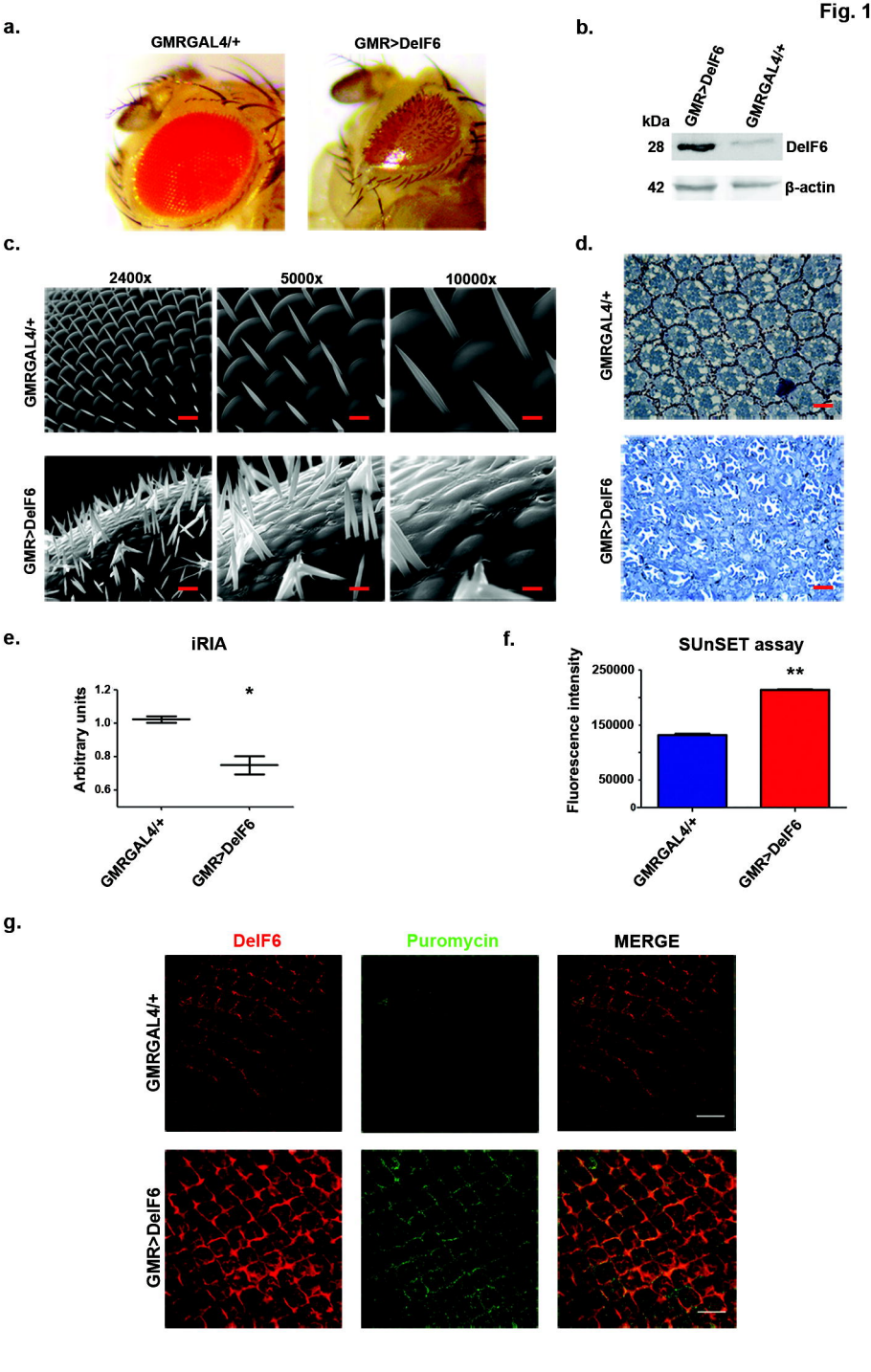
a.
GMRGAL4/+
GMR>DelF6
b.
kDa
GMR>DelF6
GMRGAL4/+
28
DelF6
42
β-actin
c.
2400x
5000x
10000x
GMRGAL4/+
GMR>DelF6
d.
GMRGAL4/+
GMR>DelF6
e.
iRIA
Arbitrary units
1.2
1.0
0.8
0.6
*
GMRGAL4/+
GMR>DelF6
f.
SUnSET assay
Fluorescence intensity
250000
150000
50000
0
**
GMRGAL4/+
GMR>DelF6
g.
DelF6
Puromycin
MERGE
GMRGAL4/+
GMR>DelF6

Fig. 2

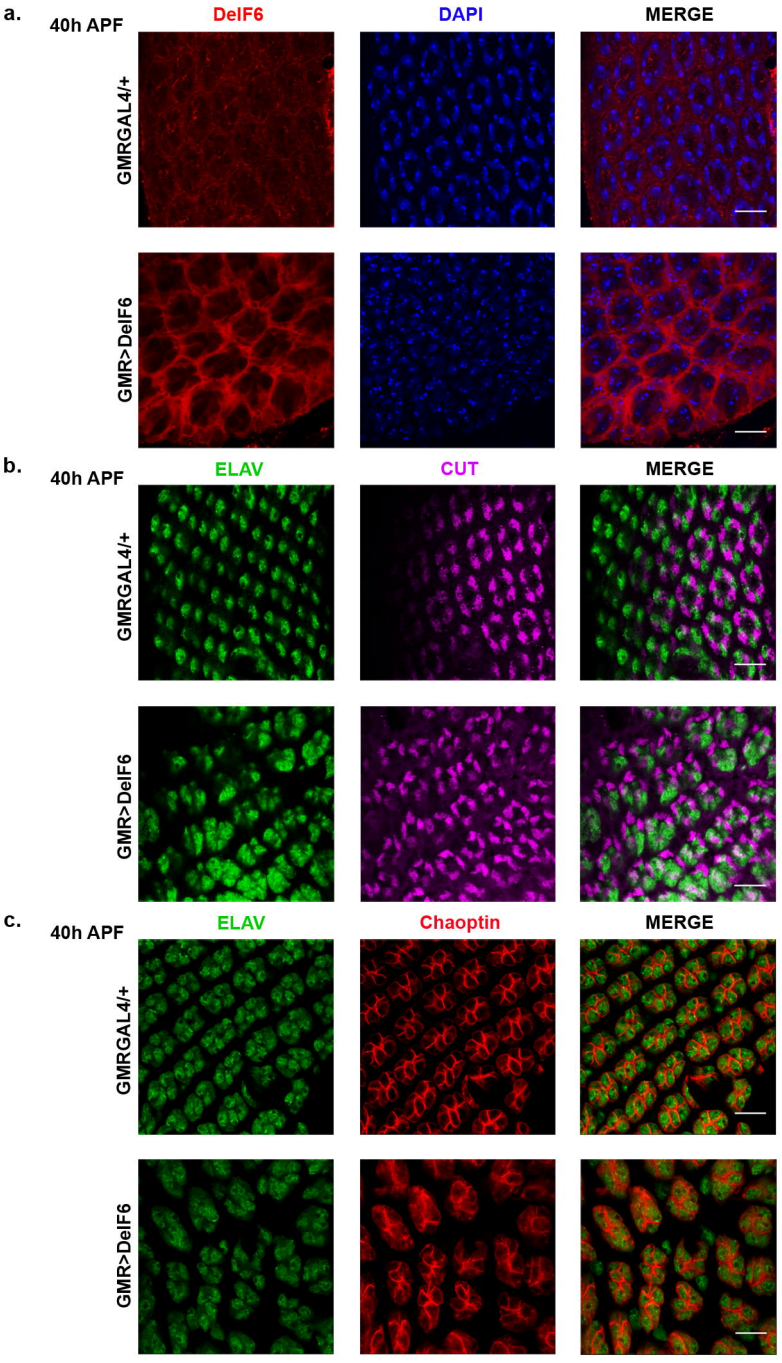
a.
40h APF
DelF6
DAPI
MERGE
GMRGAL4/+
GMR>DelF6
b.
40h APF
ELAV
CUT
MERGE
GMRGAL4/+
GMR>DelF6
c.
40h APF
ELAV
Chaoptin
MERGE
GMRGAL4/+
GMR>DelF6

Fig. 3

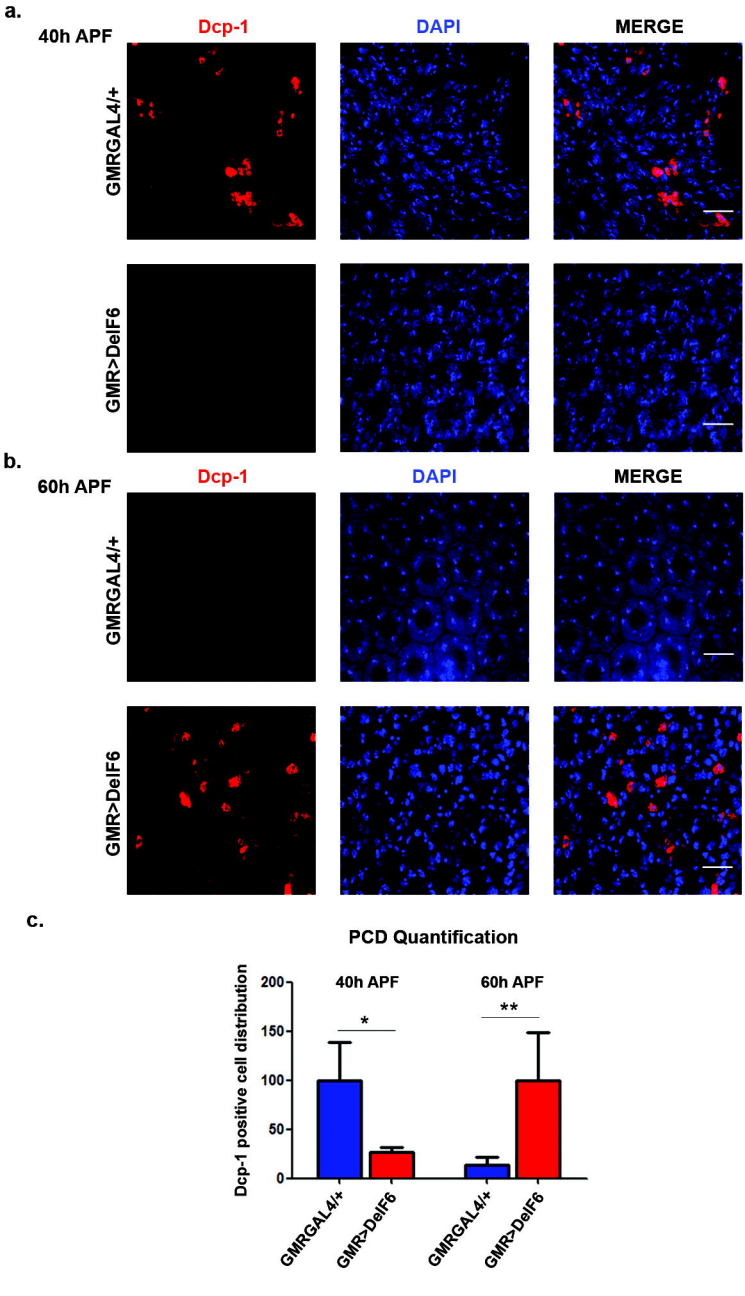
a.
40h APF
Dcp-1
DAPI
MERGE
GMRGAL4/+
GMR>DelF6
b.
60h APF
Dcp-1
DAPI
MERGE
GMRGAL4/+
GMR>DelF6
c.
PCD Quantification
Dcp-1 positive cell distribution
200
150
100
50
0
40h APF
60h APF
*
**
GMRGAL4/+
GMR>DelF6
GMRGAL4/+
GMR>DelF6

Fig. 4

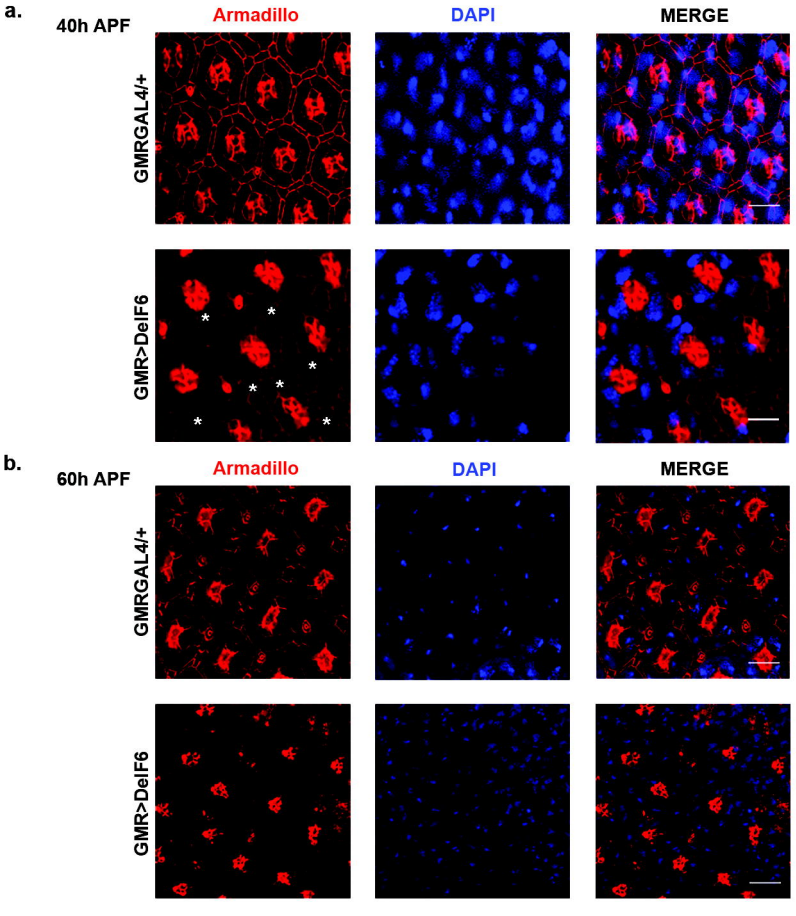
a.
40h APF
Armadillo
DAPI
MERGE
GMRGAL4/+
GMR>DelF6
b.
60h APF
Armadillo
DAPI
MERGE
GMRGAL4/+
GMR>DelF6

Fig. 5

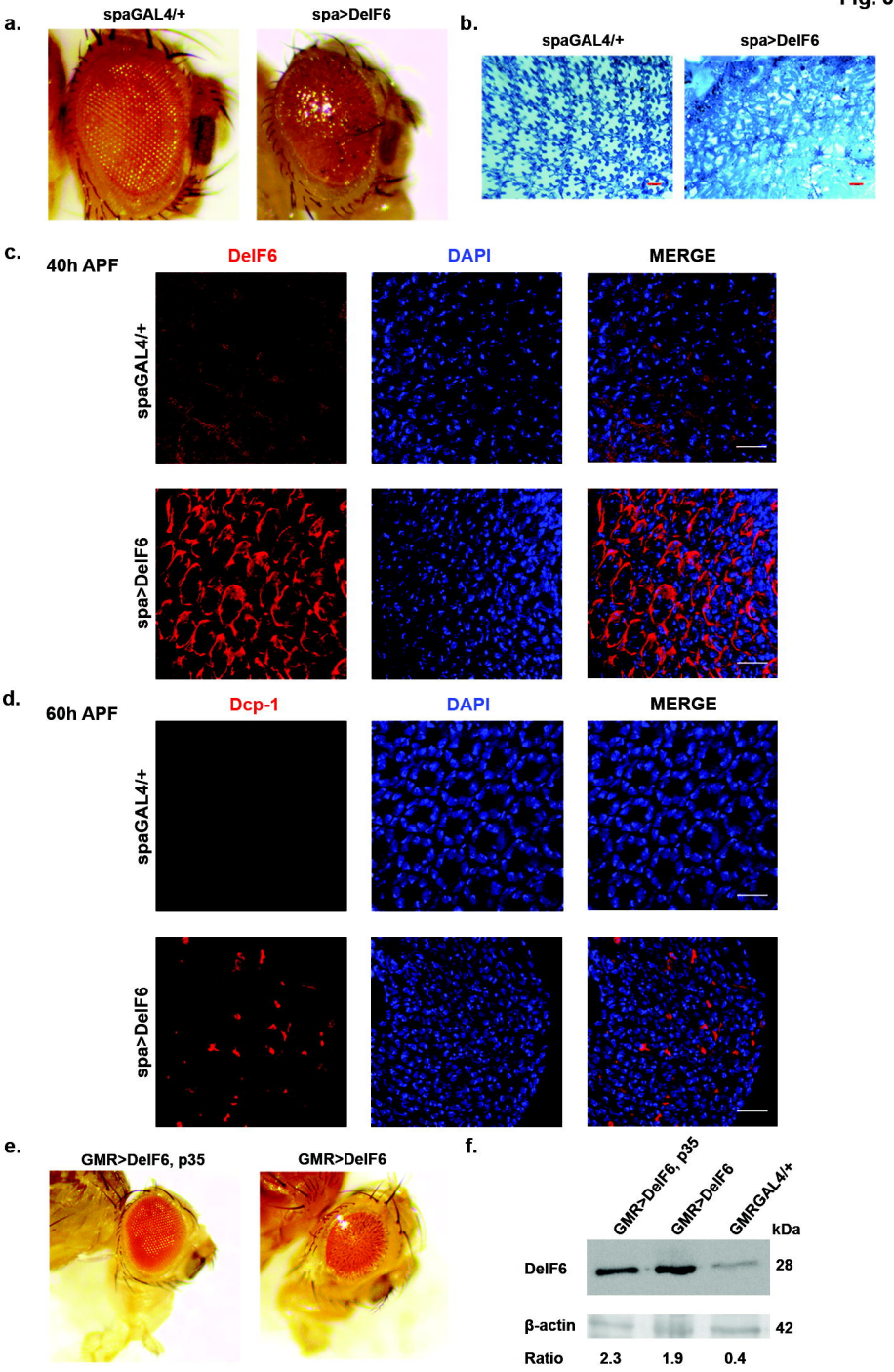
a.
spaGAL4/+
spa>DelF6
b.
spaGAL4/+
spa>DelF6
c.
40h APF
DelF6
DAPI
MERGE
spaGAL4/+
spa>DelF6
d.
60h APF
Dcp-1
DAPI
MERGE
spaGAL4/+
spa>DelF6
e.
GMR>DelF6, p35
GMR>DelF6
f.
GMR>DelF6, p35
GMR>DelF6
GMRGAL4/+
kDa
DelF6
28
β-actin
42
Ratio
2.3
1.9
0.4

a.

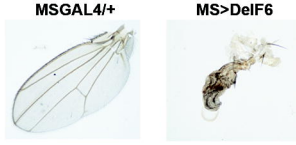
MSGAL4/+
MS>DelF6

b.

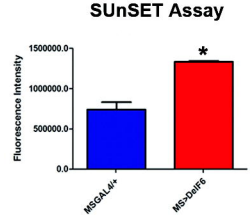
SUnSET Assay
Fluorescence Intensity
1500000.0
1000000.0
500000.0
0.0
*
MSGAL4/+
MS>DelF6

c.

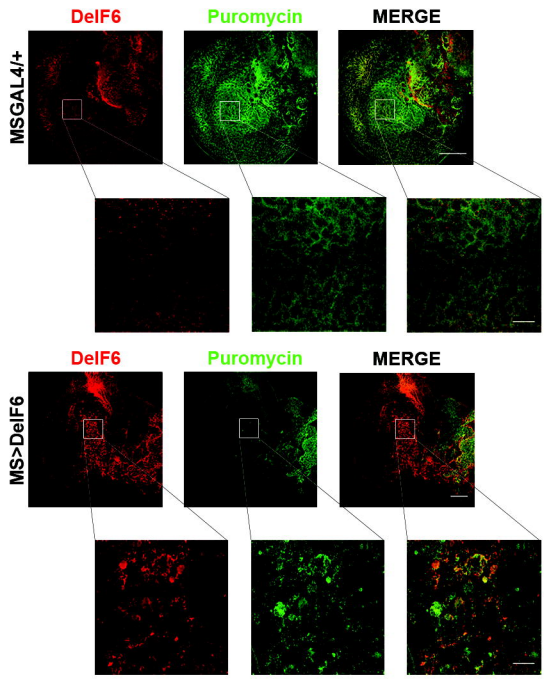
DelF6
Puromycin
MERGE
MSGAL4/+
DelF6
Puromycin
MERGE
MS>DelF6

d.

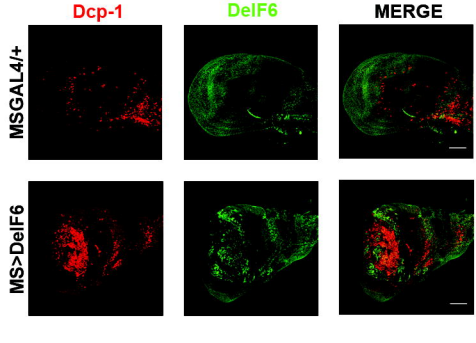
Dcp-1
DelF6
MERGE
MSGAL4/+
MS>DelF6

Fig. 7

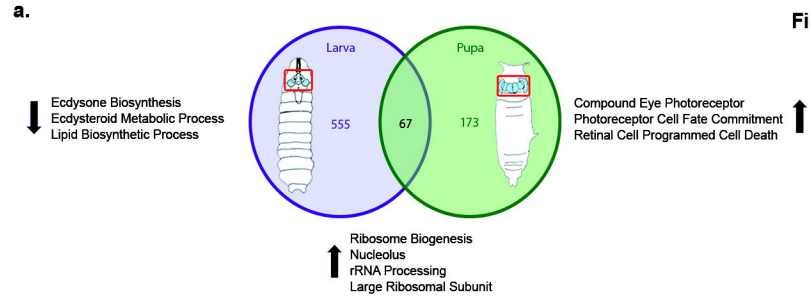
a.
Larva
Pupa
555
67
173
Ecdysone Biosynthesis
Ecdysteroid Metabolic Process
Lipid Biosynthetic Process
Compound Eye Photoreceptor
Photoreceptor Cell Fate Commitment
Retinal Cell Programmed Cell Death
Ribosome Biogenesis
Nucleolus
rRNA Processing
Large Ribosomal Subunit

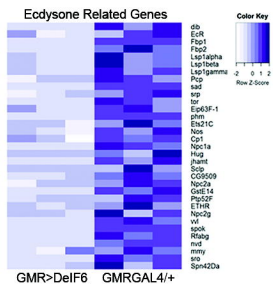
b.
Ecdysone Related Genes
Color Key
Row Z-Score
db
EcR
Fbp1
Fbp2
Lsp1alpha
Lsp1beta
Lsp1gamma
Pcp
sad
srp
tor
Eip63F-1
phm
Btk21C
Nos
Cp1
Npc1a
Hug
Jhamt
Scb
CG9509
Npc2a
GstE14
Ptp52F
ETHR
Npc2g
vvl
spok
Rfabg
nvd
mmy
sro
Spn42Da
GMR>DelF6
GMRGAL4/+

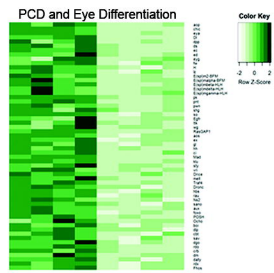
c.
PCD and Eye Differentiation
Color Key
Row Z-Score
GMR>DelF6
GMRGAL4/+

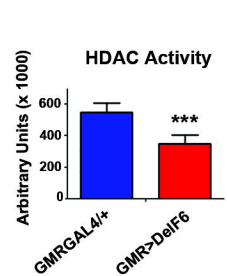
d.
HDAC Activity
Arbitrary Units (x 1000)
600
400
200
0
***
GMRGAL4/+
GMR>DelF6

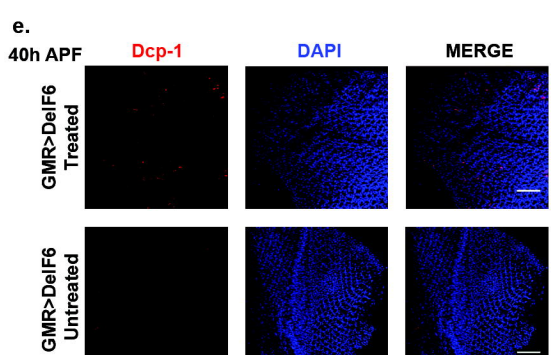
e.
40h APF
Dcp-1
DAPI
MERGE
GMR>DelF6
Treated
GMR>DelF6
Untreated

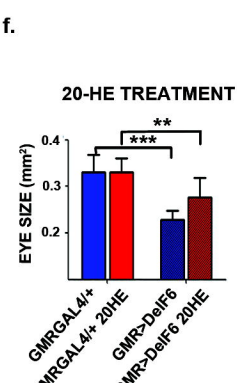
f.
20-HE TREATMENT
**
***
EYE SIZE (mm²)
0.4
0.3
0.2
GMRGAL4/+
GMRGAL4/+ 20HE
GMR>DelF6
GMR>DelF6 20HE

Fig. 8

DelF6 levels

Increased Translation

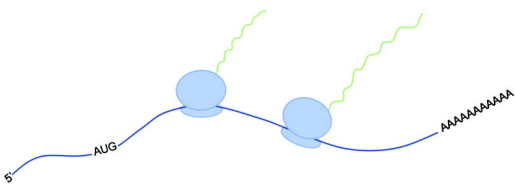

Transcriptional Rewiring

Ecdysone Biosynthesis

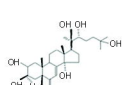

HDAC activity

Apoptosis